REVIEWS

Journal of Semiconductors
(2020) 41, 011901
doi: 10.1088/1674-4926/41/1/011901

Strain tunable quantum dot based non-classical photon sources

Jingzhong Yang, Michael Zopf, and Fei Ding†

Institute of Solid State Physics, Leibniz University of Hannover, Hannover 30167, Germany

Abstract: Semiconductor quantum dots are leading candidates for the on-demand generation of single photons and entangled photon pairs. High photon quality and indistinguishability of photons from different sources are critical for quantum information applications. The inability to grow perfectly identical quantum dots with ideal optical properties necessitates the application of post-growth tuning techniques via e.g. temperature, electric, magnetic or strain fields. In this review, we summarize the state-of-the-art and highlight the advantages of strain tunable non-classical photon sources based on epitaxial quantum dots. Using piezoelectric crystals like PMN-PT, the wavelength of single photons and entangled photon pairs emitted by InGaAs/GaAs quantum dots can be tuned reversibly. Combining with quantum light-emitting diodes simultaneously allows for electrical triggering and the tuning of wavelength or exciton fine structure. Emission from light hole exciton can be tuned, and quantum dot containing nanostructure such as nanowires have been piezo-integrated. To ensure the indistinguishability of photons from distant emitters, the wavelength drift caused by piezo creep can be compensated by frequency feedback, which is verified by two-photon interference with photons from two stabilized sources. Therefore, strain tuning proves to be a flexible and reliable tool for the development of scalable quantum dots-based non-classical photon sources.

Key words: quantum dot; entangled photons; strain tuning; piezoelectric crystal; fine structure splitting; on-chip

Citation: J Z Yang, M Zopf, and F Ding, Strain tunable quantum dot based non-classical photon sources[J]. *J. Semicond.*, 2020, 41(1), 011901. http://doi.org/10.1088/1674-4926/41/1/011901

1. Introduction

The on-demand generation of single photons and entangled photon pairs are of fundamental interest for many applications such as quantum repeaters[1–3], quantum computing[4, 5], quantum cryptography[6, 7] and quantum metrology[8–10]. Photons as quantum bits exhibit long coherence time and can travel long distances while only weakly interacting with the environment[11–13]. In the past 20 years, sources based on spontaneous parametric down-conversion (SPDC)[14–16] in the non-linear optical crystal have been the workhorse in optical quantum information science[8, 9]. Several proof-of-principle experiments have been carried out with these sources such as quantum teleportation[17–22], entanglement swapping[23–26], entanglement purification[27] or cluster/GHZ state[28–31] generation. However, there is a fundamental limit to the brightness of SPDC sources: due to their Poissonian emission characteristics, a tradeoff between single-photon purity and source efficiency has to be made. This is an inherent shortcoming for real-world applications because photon emission at the push of a button is a critical requirement in complex quantum protocols.

Semiconductor quantum dots (QDs) are the most promising candidate to generate single photons and entangled photon pairs truly on-demand. These so-called 'artificial atoms' exhibit discrete electronic states with excitonic transitions, providing means for high efficiency, deterministic emission[25, 26, 32, 33]. Moreover, the QDs are highly scalable since they are readily integrable with established semiconductor technology. In contrast to the emission of natural atoms[34, 35], QDs do not only allow for optically[36] or electrically[37, 38] excitation, they also obviate the need for bulky and complex setups. Furthermore, it is possible to integrate these entangled photon sources on-chip to make them scalable for distributed quantum networks[39, 40]. Several breakthroughs in the optical quality and photon extraction efficiency of QDs have allowed their implementation in entanglement swapping schemes at atomic quantum memory wavelengths[41]. Although alternative solid-state emitters such as color centers in diamond or defects in two-dimensional materials are being investigated, they each exhibit different drawbacks with regard to the emission quality, such as low quantum efficiency or low photon coherence[42, 43].

However, 'no two snowflakes are alike' is a principle that also seems to hold for QDs. Their growth is governed by randomness in shape, material composition, and internal strain fields. This inability to grow perfect QDs is a major challenge: As an example, key elements in quantum information processing[44–47] such as two-photon interference (TPI) require photons from different sources to be indistinguishable. Furthermore, due to anisotropies in the QD confinement potential, the exciton degeneracy is lifted[48]. In time-integrated measurements, the resulting fine-structure splitting (FSS)[49–51] will significantly decrease the degree of entanglement of photon pairs steaming from the biexciton-exciton radiative cascade[52, 53]. QDs grown by molecular-beam epitaxy (MBE)[54] have so far shown the greatest potential for quantum information applications due to their high reproducibility and photon coherence. In order to modify the electronic and optical properties of QDs to e.g. counteract the broad emission wavelength distribution, several post-growth tuning techniques were exploited, such as in-situ thermal annealing[55, 56], magnetic field[57] or electric fields[37, 58]. However, thermal an-

Correspondence to: F Ding, f.ding@fkp.uni-hannover.de
Received 30 SEPTEMBER 2019.

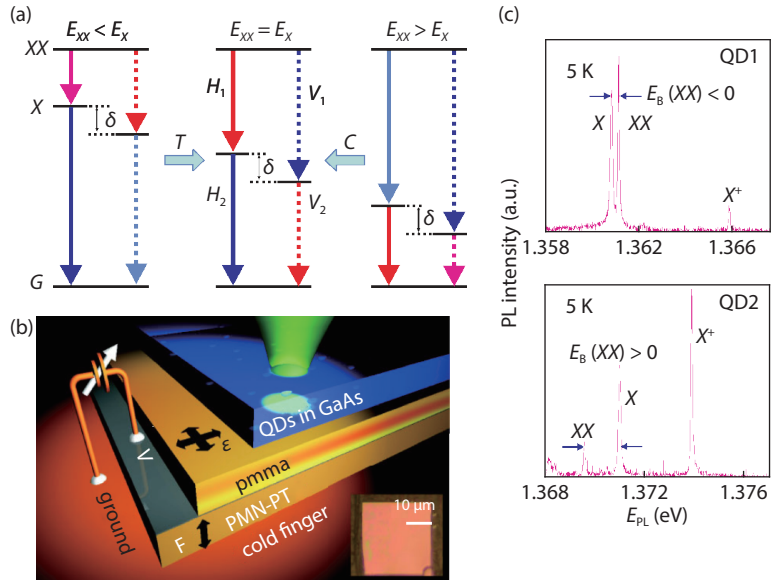

Fig. 1. (Color online) (a) Scheme of the cascade emission of the *XX*. The solid (dashed) line represents the *XX* decay path by emitting *H*(*V*) polarized photons. By applying tensile or compressive strain, the $E_B(XX)$ energy of *XX* relative to *X* can be robustly adjusted. (b) Schematic of the device used for strain tuning of InGaAs/GaAs QDs, as located on the cold figure of a liquid He cryostat. Both the laser excitation and photon collection are performed by a photoluminescence setup above the device. The inset shows a 200 nm-thick QD containing nanomembrane. (c) Low-temperature PL spectrum with different $E_B(XX)$. The emission line lying on the higher energy side of *X* and *XX* in both spectra is attributed to the positive trion X^+ emission. Reprinted figure with permission from Ref. [60]. Copyright 2019, the American Physical Society.

nealing is irreversible and coarse, while magnetic field tuning usually requires bulky equipment unsuitable for scalable applications. Electric field tuning based on the quantum-confined Stark effect[59] is promising but prevents the implementation of electrical excitation of QDs.

In this review, we recapitulate the development and achievements for the strain tuning of III–V QDs. We start by introducing the effect of external biaxial stress on a QDs containing nanomembrane placed on a piezoelectric actuator[60, 61]. The QDs emission wavelength changes proportionally with the applied voltage to the actuator. In combination with diode structures, QDs can be triggered electrically to emit wavelength tunable single photons and entangled pairs[61–65]. These hybrid devices also allow for independent tuning of wavelength and decay time. Light-hole exciton emission from QDs has been tuned[66, 67] via strain, allowing for on-chip quantum circuit construction[68–70] due to the in-plane photon emission. QD containing nanostructures such as nanowires[70–72] have been successfully integrated with piezoelectric actuators. This approach may be readily extended to versatile nanostructures such as circular Bragg gratings[73–75], or micropillars[76]. The advantage of the strain tunability of semiconductor QDs comes with the challenge of piezo creep[77], resulting in e.g. wavelength drifts after applying a DC voltage to the piezo actuator. This effect may be counteracted using frequency feedback, allowing for time-stable TPI of photons from separated, stabilized emitters. Strain tuning thus proves a versatile tool that is ready for use in real-world quantum applications[78].

2. Strain-engineering of semiconductor quantum dots

To understand the energy band structure and optical properties of semiconductors, *k*·*p* perturbation theory is commonly employed[79]. The band structure of a semiconductor is modified under a uniform deformation of the semiconductor caused by the internal or external stress. The effect of strain on the Hamiltonian was investigated by Pikus and Bir in the 1960s[80, 81]. The changes observed in semiconductor lattices subject to strain fields allow manipulating the excitonic states and optical emission features of semiconductor QDs.

Fig. 1 shows the effect of strain on InGaAs/GaAs QDs attached to a biaxial piezoelectric actuator that induces. The QD sample is grown by MBE along the [001] crystal direction on a GaAs substrate. The self-assembled InGaAs QDs are embedding in layers of GaAs, grown on top of AlGaAs sacrificial layer. Square patterns are defined in the sample by photolithography. Making use of the selective etching of the sacrificial layer with diluted hydrofluoric acid, the nanomembranes are released and become free-standing on the substrate. They are then transferred on a 300 μm thick piezoelectric $[Pb(Mg_{1/3}Nb_{2/3})O_3]_{0.72}$-$[PbTiO_3]_{0.28}$ (PMN-PT), allowing for the application of large, biaxial in-plane strain fields at low temperature. As illustrated in Fig. 1(b), PMMA is used as an adhesive layer between the QD membranes and the piezoceramic[82–84]. Fig. 1(a) shows the effect of biaxial strain on the electronic structure in the QD: The biexciton (*XX*) radiatively decays to the intermediate exciton (*X*) states with lifted degeneracy. The *X* states will then decay to the ground state (*G*) under the emission of another photon[85]. While the compressive (tensile) strain is applied on the nanomembrane, the neutral *X* emission presents a blue- (red-) shift while the FSS (δ) stays constant. Fig. 1(c) shows the photoluminescence (PL) spectra of the neutral *X*, *XX* and positive trion X^+ emission at a temperature of 5 K. In the experiment, QD1 and QD2 are defined as negative and positive depending on the energy difference (E_B) between *X* and *XX* photon emission, corresponding to *XX* transition line located at the right and left side

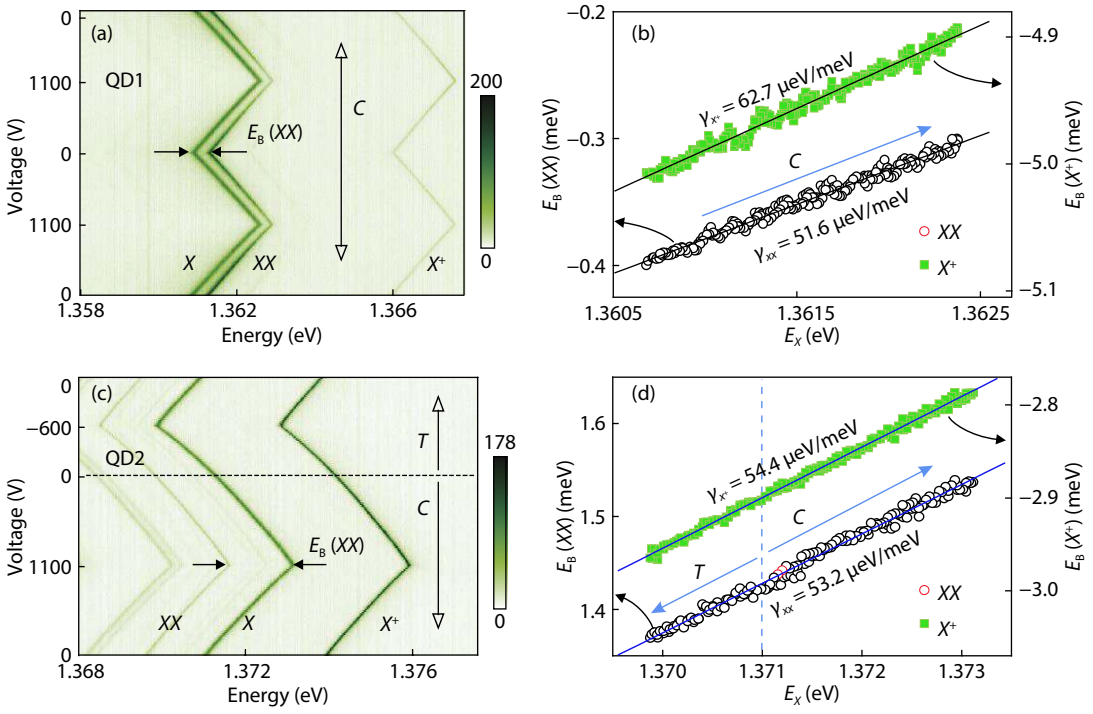

Fig. 2. (Color online) PL spectra of (a) QD1 and (c) QD2 as a function of applied voltage on the PMN-PT actuator. The linear increase of $E_B(XX)$ and $E_B(X^+)$ with E_X for both QD1 and QD2 are shown in (b) and (d). Reprinted figure with permission from Ref. [60]. Copyright 2019, the American Physical Society.

of X photon emission respectively. (These three emissions are distinguished by power-dependent and polarization-dependent photoluminescence measurements)[86–88].

In Figs. 2(a) and 2(c), the PL spectra of QD1 and QD2 are shown as a function of the voltage applied to the PMN-PT actuator. The voltage is swept between 0 to 1100 V with steps of 20 V. When the voltage is positive, an in-plane compressive strain is always applied on the QDs membrane, resulting in a blueshift of up to ~1.8 meV. Then, the effect of biaxial strain on the binding energy binding energies $E_B(XX)$ and $E_B(X^+)$ relative to X is investigated for the different dots. As shown in Figs. 2(b) and 2(d), both the $E_B(XX)$ and $E_B(X^+)$ monotonically increase with a constant slope while the X emission is blue shifted. By means of empirical pseudopotential calculations, this effect is attributed to an increase in electron-hole Coulomb interaction upon compressive biaxial stress. Furthermore, the FSS keeps constant while tuning the voltage, as confirmed by the calculations[89].

Therefore, biaxial strain tuning is a reliable method to engineer the QD electric structure in a precise and reversible way. Excitonic emission wavelengths are controlled and color coincidence between X and XX photons can be achieved. The possibility to tune the photon emission wavelength can resolve the scalability difficulty via the specific strain applied to the different QD sources. On the other hand, the demonstration of strain tuning also contributes to the investigation of other material systems such as 2D graphene[90], quantum dot molecule[91] or silicon-vacancy center in diamond[92], allowing for the fabrication of advanced single and entangled photon sources.

3. Wavelength tuning of single photons from a light emitting diode

Semiconductor QDs have the inherent advantages of integrability with the mature semiconductor technologies that have matured in the research and industry. Electrically driven single-photon sources (SPs) based on QDs helps to simplify the bulky laser excitation system and make QDs more valuable for the use in on-chip quantum devices[93–95]. In SPDCs wavelength tunability of the emission can be easily achieved by using identical bandpass filters[96, 97]. However, due to the stochastic growth process, different QDs usually emit photons at different wavelengths. Strain tuning technique has been verified to be a viable tool to remove this scalability obstacle for QDs in order to realize quantum communication between remote nodes[12, 98, 99].

Fig. 3(a) shows the sketch of a wavelength-tunable, electrically triggered light-emitting diode (LED) device containing InGaAs/GaAs QDs grown by MBE. The QDs are embedded between a n- and p- doped GaAs layers. Nanomembranes are fabricated and transferred on the PMN-PT via gold-gold thermo-compression bonding, allowing for the application of in-plane biaxial strain on the QDs. The electric triggering is implemented by applying a DC bias V_d and a 300 ps consecutive electrical pulse V_{pp} (see Fig. 3(c)). Another DC bias V_p is applied to the piezoelectric actuator, sharing a common ground connection with the triggering part. A microscope objective is located on top of the sample and collects the emitted photon emission. A sketch of the complete device is illustrated in Fig. 3(a). The microscope image in Fig. 3(b) shows the electrical bonding on top of the n-GaAs nanomembrane via aluminum wires[82, 83].

A sequence of optical characterization measurements is implemented to demonstrate that this LED allows for adjusting the wavelength of photon emission which is effectively triggered by ultrashort electric pulses. Fig. 3(d) shows a group of electroluminescence (EL) spectra for different DC voltage amplitude. The emission peaks are distinguished with

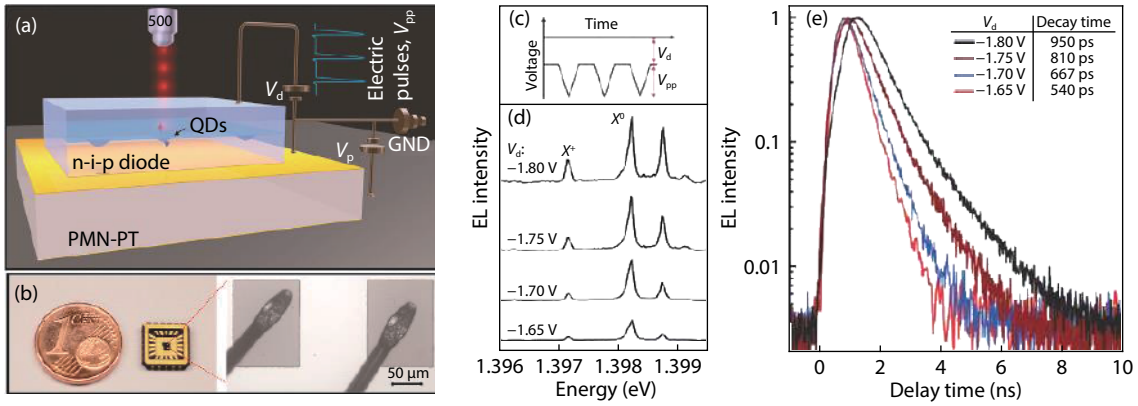

Fig. 3. (Color online) Sketch and characterization of a nanomembrane-based strain tunable single- photon-emitting diode. (a) n–i–p diode nanomembrane containing InGaAs/GaAs QDs bonded on a PMN-PT crystal via gold-to-gold thermo-compression bonding. The p-contact of the nanomembrane and the PMN-PT share a common ground. A diode voltage V_d and piezo voltage V_{pp} can be applied independently. (b) Microscope image of the strain tunable single-photon LED device. (c) The electric pulse applied on the nanomembrane is composed of two parts, the DC bias V_d and ultra-short pulse V_{pp}. (d) EL spectra from LED under different DC bias V_d. (e) Fluorescence lifetime histograms of the neutral X photon emission for different DC bias. Reprinted with permission from Ref. [61]. Copyright 2013, American Chemical Society.

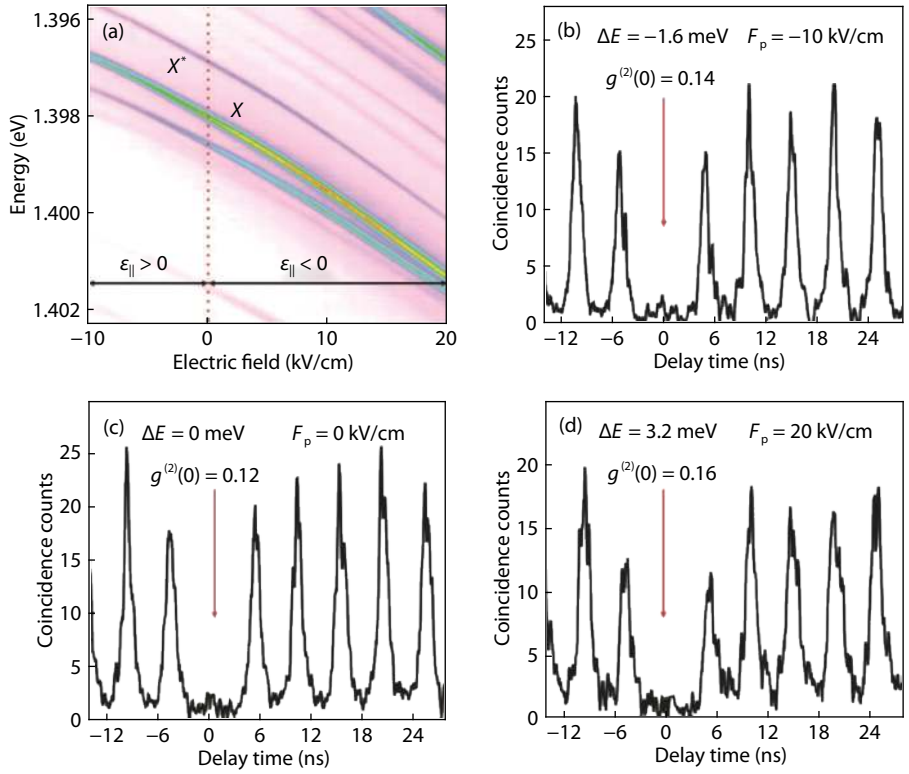

Fig. 4. (Color online) (a) Tunable X photon emission line under in-plane biaxial strain $\varepsilon_{||}$. (a) $\varepsilon_{||} < 0$ (compressive) and $\varepsilon_{||} > 0$ (tensile) strain is obtained for positive and negative electric fields applied to the PMN-PT substrate, respectively. (b)–(d) Autocorrelation measurements are implemented with the X emission, and the suppression of coincidence counts at zero-time confirm the single-photon emission when varying the strain is applied to the QDs. Reprinted with permission from Ref. [61]. Copyright 2013, American Chemical Society.

polarization-resolved EL measurements. It is also apparent that the decay time of X photon emission gets altered with the changing of V_d (Fig. 3(e)). This is ascribed to the reduced time jitter at a low DC bias because of the band bending[100–102]. More specifically, the quantum tunneling effect introduces an additional fast, non-radiative decay channel to the bright excitonic recombination in the QD.

Apart from the investigation of electrically triggered QDs, their strain tunability in the nanomembrane is also studied, while keeping the single-photon emission properties. In Fig. 4(a), the EL-spectrum series as a function of different electric field F_p is implemented by controlling the voltage V_p. The X photon emission line shows a blueshift with the F_p changed from −10 to 20 kV/cm. To demonstrate single-photon emission, the second-order autocorrelation function $g^{(2)}(\tau)$ is measured for the X emission and shown in Figs. 4(b)–4(d). As evident from the results, the single-photon purity is maintained under different strain conditions at the QD. Therefore, electrically triggered QDs can provide a stable single-photon emission with a precisely adjustable wavelength.

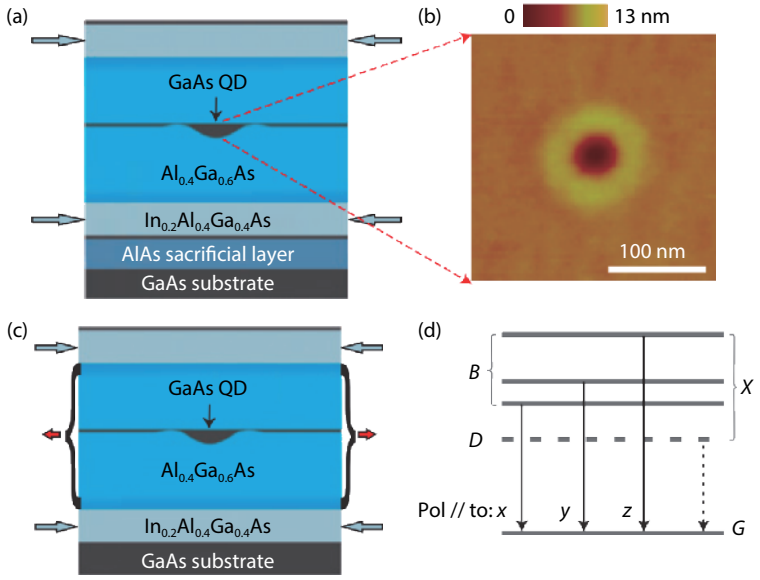

Fig. 5. (Color online) (a) Schematic of the GaAs QDs heterostructure in the GaAs substrate, the length of the arrows are indicating the magnitude of in-plane strain. (b) Atomic force microscopy (AFM) image of a droplet-etched nanohole on the AlGaAs surface before GaAs filling. (c) Schematic of the GaAs QDs heterostructure after the etching of the AlAs sacrificial layer. (d) The energy level of the dipole transition in the QDs. *X* represents the light hole exciton, which is composed of a dark state (D) and three bright states (B). *x* and *y* denote the in-plane crystal direction and *z* denotes the out-plane direction. Reprinted with permission from Ref. [66]. Copyright 2013, Springer Nature.

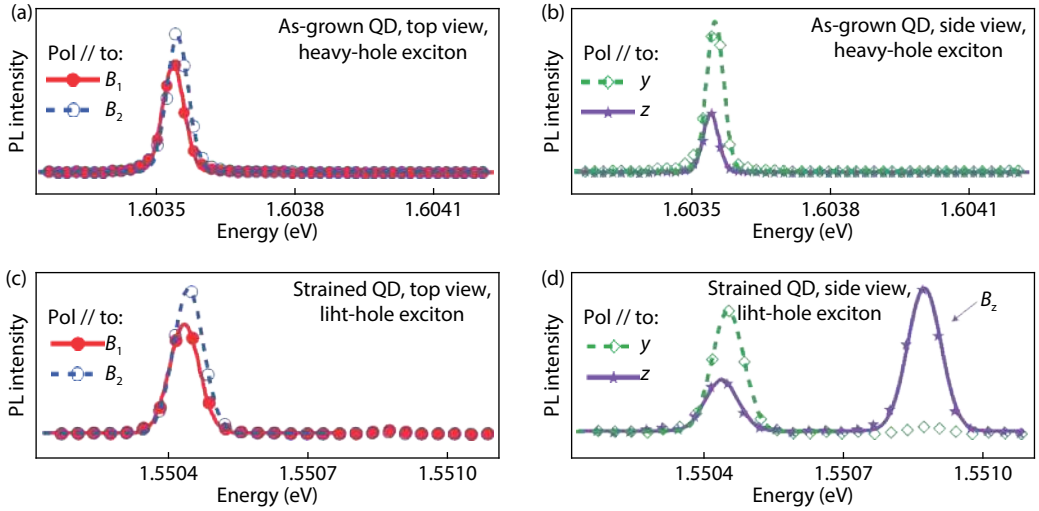

Fig. 6. (Color online) PL spectra of a heavy hole and light hole exciton in GaAs/AlGaAs QDs. In (a) and (c), the open and filled circles represent the two perpendicular in-plane polarized components of light along the B_1 line has the polarization close to the *x*-direction [110]. In (b) and (d) the light is collected from the cleaved edge of the sample, the open diamond line has the polarization close to the *y*-direction [$1\bar{1}0$]. Besides, there is an additional emission at higher energy in (d) indicting the dominated light hole exciton emission. Reprinted with permission from Ref. [66]. Copyright 2013, Springer Nature.

4. Strain tuning of light-hole excitons

Semiconductor QDs predominantly allow for the formation of excitonic complexes based on heavy-holes. In contrast, light-hole excitons are quasiparticles formed by a single electron and a light hole[103, 104]. It features an in-plane photon emission, making it suitable for application as an on-chip photon source. Besides, light-hole excitons allow for mapping of photon polarization to electron spin[105], control of the light-hole spin state with microwave field[106] or tomography measurements on the electron spin state in semiconductor devices[107]. A light hole ground state can be obtained by applying elastic stress to initially unstrained QDs. The sketch of the heterostructure is shown in Fig. 5(a). In-plane anisotropy of the confinement potential is expected to contribute to light-hole-heavy-hole mixing[108–111]. The sample, containing highly symmetric GaAs/AlGaAs QDs is grown by MBE[112] and is based on nanohole etching and infilling. An atomic force microscope image of a hole etched on AlGaAs is shown in Fig. 5(b). By etching the underlying AlAs sacrificial layer, the biaxial tensile strain on the QDs embedded in the membrane, resulting in a light hole ground state.

Photoluminescence measurements are carried out to investigate the emission of the light hole exciton. Comparing Figs. 6(a) and 6(b), it is seen that two in-plane polarized light components are collected from the top of the sample along *z*-direction [001]. When the signal is collected from the side

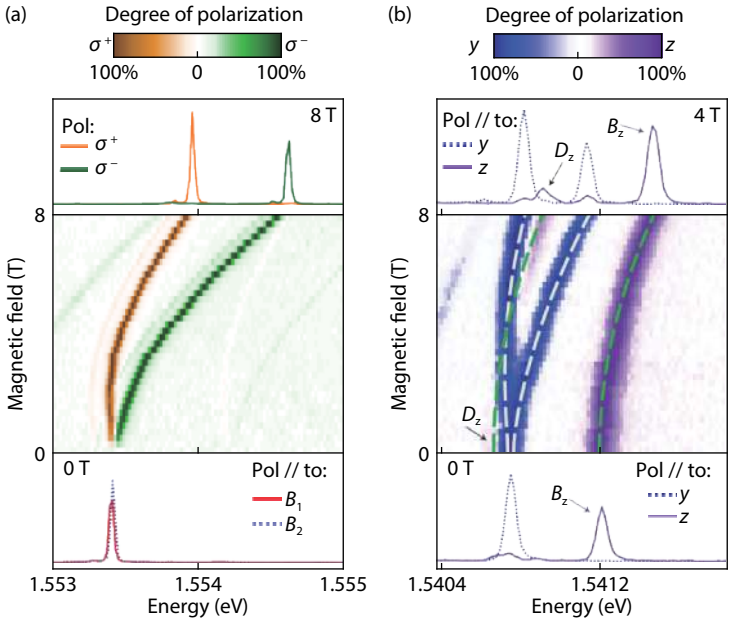

Fig. 7. (Color online) Polarization-resolved PL spectra of the light hole exciton emission independence of a magnetic field applied in the *z*-direction. Emission spectra are collected along *z*-direction (a) and *x*-direction (b). The dashed lines in (b) represent fits of the peak positions for the in-plane polarized B_1 and B_2 lines (white) and *z*-polarized B_z and D_z lines (green). Reprinted with permission from Ref. [66]. Copyright 2013, Springer Nature.

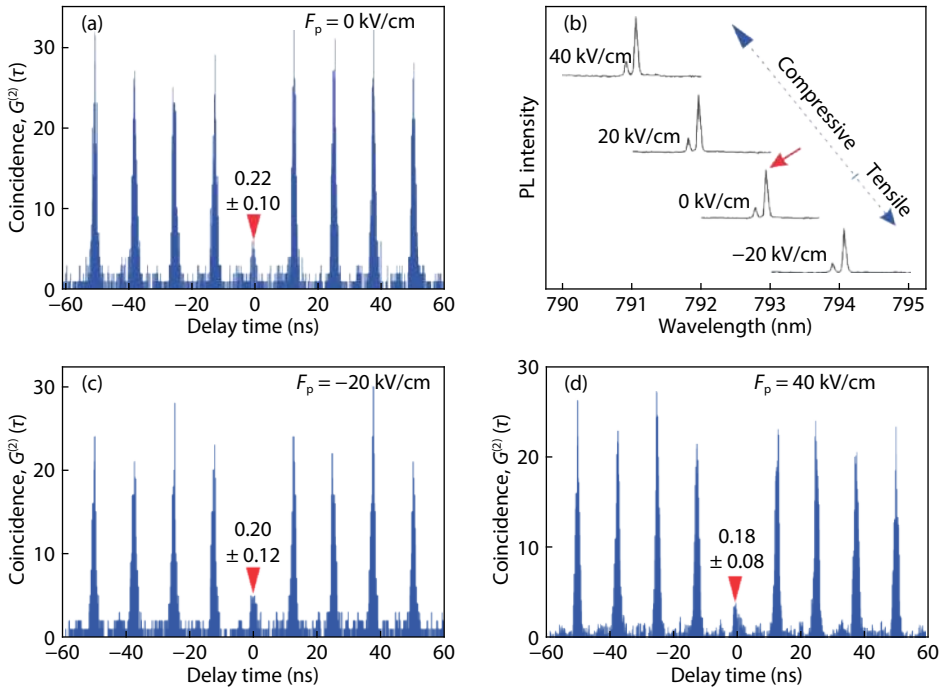

Fig. 8. (Color online) (a) Autocorrelation measurement of light hole exciton emission without any strain applied by PMN-PT. (b) Light hole exciton emission wavelength as a function of applied electric field on PMN-PT. Autocorrelation measurements (c) and (d) of the light hole emission, conducted at different electric field F_p. Reprinted with permission from Ref. [67]. Copyright 2015, American Chemical Society.

view of the sample (Figs. 6(c) and 6(d)) along the *x*-direction [110], there is a strong peak appearing at a higher energy for strained QDs illustrating the generation of the light hole exciton.

To confirm that the observed emission is from the light hole exciton, a magnetic field is applied along the *z*-direction. Fig. 7(a) shows the polarization-resolved spectra of a single QD independence of the magnetic field. The two peaks start to shift and split further with increasing field magnitude owing to the Zeeman effect. In Fig. 7(b), the polarization-resolved spectra are obtained along the *x*-direction, revealing the dark exciton state as the field increases[113].

Now the observed light hole exciton emission is studied in dependence of strain. Single-photon emission is confirmed by second-order auto correction measurements under pulsed excitation, as shown in Fig. 8(a). Applying an electric field F_p along the out-of-plane direction of the PMN-PT crystal results in a compressive or tensile biaxial strain which

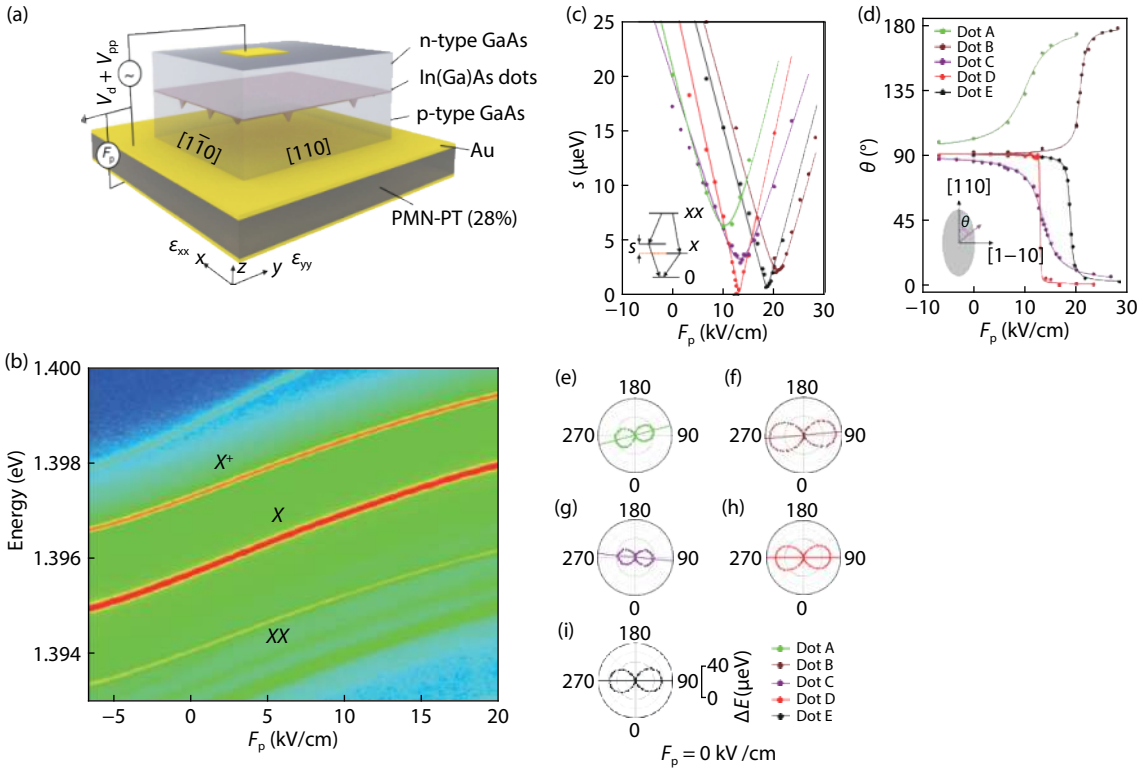

Fig. 9. (Color online) Schematic and characterization of a strain tunable entangled-light-emitting diode. (a) Sketch of the device. (b) EL emission spectra from a single QD as a function of the electric field applied to the piezoelectric actuator. (c) FSS of the exciton (*X*) state as a function of F_p for different QDs. The inset shows the biexciton cascade and FSS between *X* states. (d) *X* photon polarization angle relative to the nanomembrane crystal orientation [110] as a function of the electric field at the piezo. (e)–(i) represent the FSS and polarization angle of different QDs at zero electric fields F_p. Figure is taken from Ref. [65] without changes are made. CC BY[119].

is transferred to the nanomembrane and therefore causes an emission wavelength shift (Fig. 8(b)). Auto correlation measurements under different electric fields applied to the PMN-PT substrate are performed. From Figs. 8(c) and 8(d), we can see there is no apparent change in $g^{(2)}(0)$ at different strain conditions. This shows that the single-photon emission character of the light hole exciton is conserved and therefore indicates that tuning of strain fields does not deteriorate the emission properties.

5. Fine structure tuning in an entangled-photon emitting diode

Entangled photon pairs are fundamental elements in several quantum information applications such as quantum communication and optical quantum computing. So far, polarization-entangled photon pairs are mainly obtained from SPDC in non-linear optical materials. However, the physical drawback of this source is the probabilistic emission, resulting in either a low source brightness or an increased number of multiple emitted pairs per excitation cycle[114, 115]. In contrast, semiconductor QDs can emit photon pairs on-demand by exploiting the *XX* cascade via the intermediate *X* state. However, the presence of an FSS, describing the lifted *X* state degeneracy, limits the polarization-entanglement, which has been a challenge for QD based entangled photon sources for over 15 years[38]. One possibility to overcome this issue is by using uniaxial strain fields. This was proposed and successfully implemented for In(Ga)As/GaAs QDs embedded in a light-emitting diode and integrated with a PMN-PT substrate. The FSS is then eliminated by uniaxial strain induced by the piezoelectric actuator, thereby reducing asymmetries in the QD confinement potential[116–118].

Fig. 9(a) shows the schematic of the device. The QDs are embedded in n–i–p nanomembranes that are bonded on PMN-PT via gold-to-gold thermo-compression bonding. The QDs are electrically triggered by a DC voltage V_d and an ultrashort electric pulse V_{pp}. Meanwhile, a bias applied to the piezoelectric actuator results in an electric field F_p by which uniaxial strain is induced in PMN-PT that is transferred to the QDs. Fig. 9(b) shows the electroluminescence (EL) spectra obtained from a single QD, showing a shifted emission wavelength as a function of the electric field applied to the PMN-PT host substrate since the semiconductor energy band gaps are modified by the induced strain.

Applying a suitable uniaxial strain to the QDs improves the symmetry of the confinement potential so that the FSS is reduced[120, 121]. Fig. 9(c) shows the relationship between the FSSs of different QDs as a function of F_p. It is possible to significantly reduce the FSS or even eliminate it when the dot's initial in-plane orientation is along the applied strain direction. With increasing F_p the *X* photon polarization rotates differently for different QDs (Fig. 9(b)). This is determined by the original orientation of the *X* photon polarization at $F_p = 0$. For QD A and B, the angle between the polarization direction of the high-energy line with respect to the [110] direction of the GaAs nanomembrane is higher than 90°. Therefore, the polarization angle increases with increasing F_p (Figs. 9(e) – 9(f)). The polarization angle changes in the opposite direction for QD C–E (Figs. 9(g)–9(i)) with initial angles

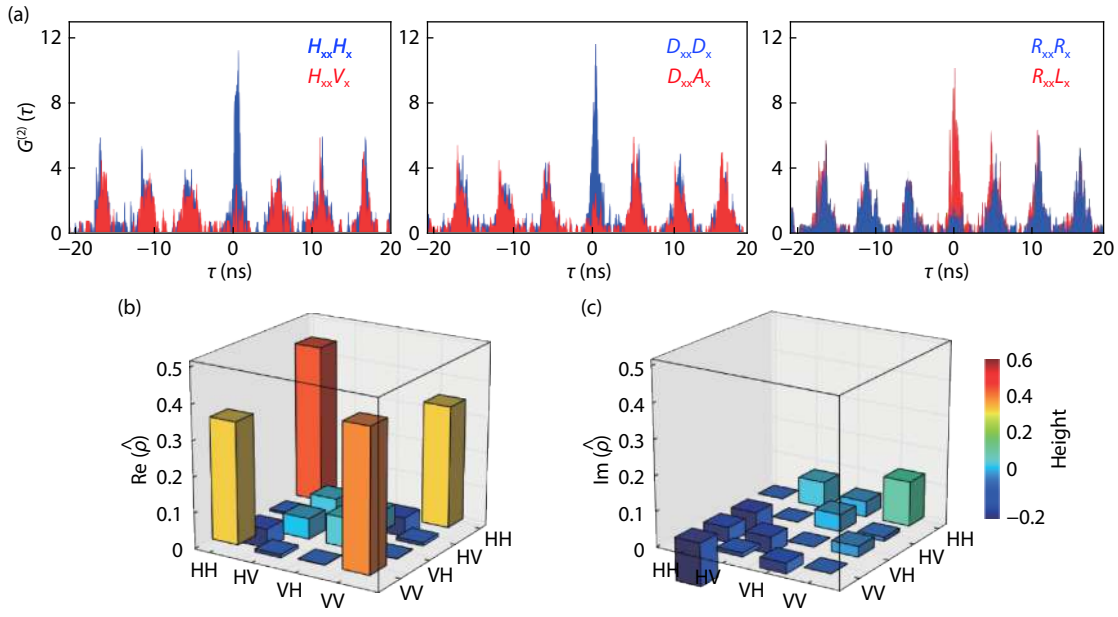

Fig. 10. (Color online) Entanglement characterization of the *XX* and *X* photons. (a) Cross-correlation measurements for co-polarized photons (blue) and cross-polarized photon (red) in different polarization projection bases H, V, D, A, R or L. (b) Real and (c) imaginary part of the two-photon density matrix, from which the degree of entanglement can is obtained. Figure is taken from Ref. [65] without changes are made. CC BY[119].

smaller than 90°.

After the reduction of the FSS, the degree of polarization-entanglement for the *XX*–*X* photon pairs is investigated. Cross-correlation measurements are conducted on these photons (Fig. 10(a)) in co- and cross-polarized bases[37, 38, 122]. The first two diagrams of Fig. 10(a) show a strong bunching behavior for *XX* and *X* photons at zero time delay for parallel polarizations (HH and DD) and an anti-bunching for perpendicular polarizations (HV and DA). The opposite behavior is observed in the third diagram for the circular polarization basis. The measurements indicate that the photon pairs emitted by the QD are found in one of the Bell states $|\varphi^+\rangle = |H_{XX}H_X\rangle + |V_{XX}V_X\rangle$ (*H* and *V* indicate the horizontal and vertical polarization of the photon, respectively). Quantum tomography is carried out to determine the density matrix of the entangled state[123] (Figs. 10(b) and 10(c)). Reducing the FSS by applying strain results in an entanglement fidelity higher than 0.75, determined from the density matrix[124]. Therefore, the strain tuning technique has been successfully proven to enable high-fidelity entangled photon emission based on semiconductor QDs.

6. Strain tuning of quantum dot containing nanowires

In quantum information processing (QIP), there are two key points for the generation of single photons, which is high brightness[125, 126] and indistinguishability[127, 128]. QDs embedded in bottom-up grown nanowires have the potential to fulfilled these requirements[129, 130]. Nanowire structures have shown high photon extraction efficiency and high coupling efficiency[131] into single-mode optical fibers due to the Gaussian emission profile[72, 132, 133]. Moreover, nanowires have been obtained with little spectral dephasing present in the QDs, allowing for coherence times up to 1.2 ns[134, 135]. However, also these structures exhibit distinguishable exciton emission wavelengths from separate emitters due to stochastic growth processes[136, 137].

The emission wavelength of InAsP QDs embedded in bottom-up grown InP nanowire can be tuned by strain, as illustrated in Fig. 11. The nanowires are placed on a PMN-PT substrate (Fig. 11(a)) and are then mounted in a He cryostat (5 K) with an objective on top for exciting the QDs. The emission of the nanowire is collected from the side. To investigate the tunability of nanowires by strain, a series of PL spectra from the exciton emission is recorded as a function of the applied voltage. Fig. 11(b) shows that the exciton emission energy is tuned by ~6.3 meV when applying tensile and compressive strain by the piezo. Afterward, the exciton emission of two nanowires placed on two independent piezo-crystals is studied. Fig. 11(c) shows PL-spectra as a function of the applied electric field on two piezoelectric crystals. With independent electric fields applied on these PMN-PT chips, it is possible to tune the emission wavelength of two QDs into resonance. Additionally, the exciton lifetimes of the two nanowires QDs are measured, showing comparable values. This indicates that the high indistinguishability of the photons from different QD sources can be obtained if spectral dephasing in the QDs is small.

The demonstration of strain tuning on nanowire QDs proves the great potential for tuning the emission of QDs embedded in nanostructures. This may facilitate quantum optical experiments such as TPI based on nano-photonic devices, and thereby advance the development of on-chip quantum technologies. One possibility is the combination of strain-tuning with nanoscale-structures that enhance the brightness or photon indistinguishability of QD based quantum light sources.

7. Wavelength tuning of polarization-entangled-photon sources

As shown above, strain-tuning enables the generation of

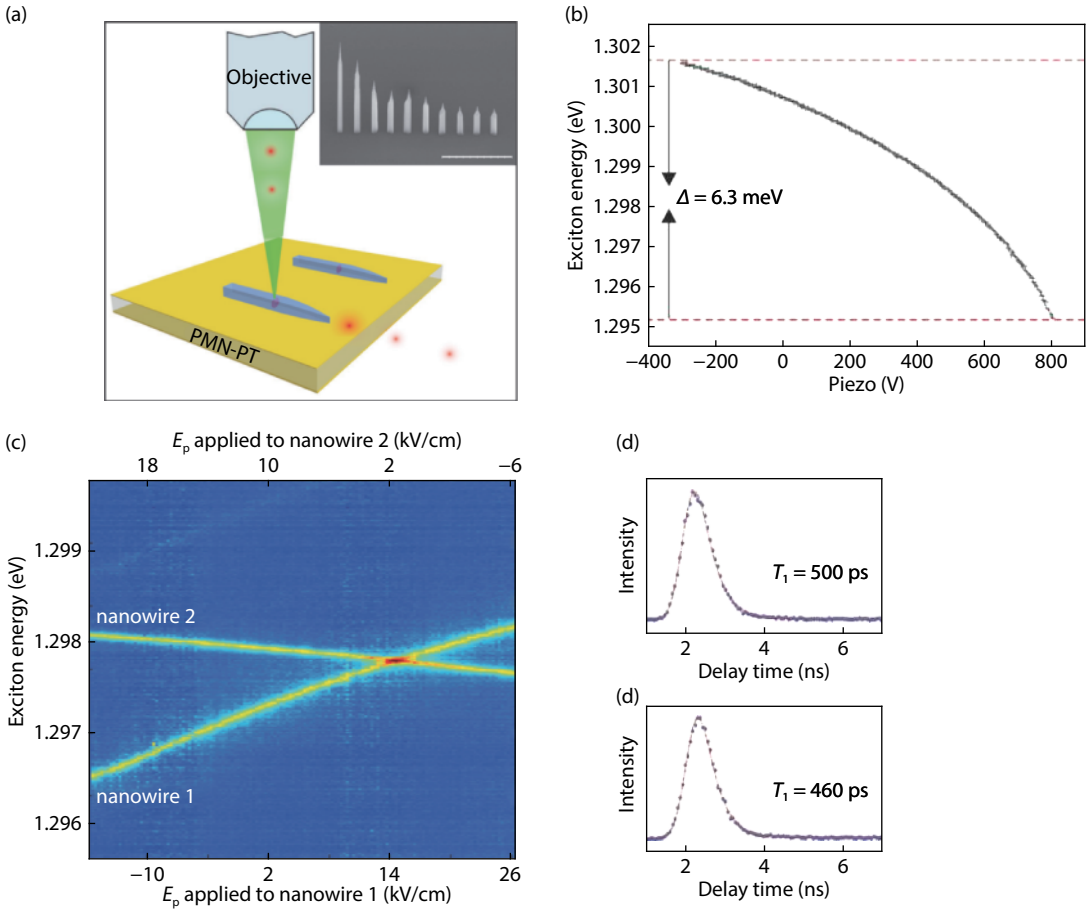

Fig. 11. (Color online) Sketch and characterization of the device allowing for strain-tuning of QD containing nanowires. (a) Sketch of InP nanowire containing InAsP QD placed on a PMN-PT substrate, and the PL setup featuring QD excitation from the top and photon collection from the side. Inset shows the scanning electron microscopy (SEM) image of the nanowires with different taper. (b) QD exciton emission energy as a function of the voltage applied to PMN-PT. (c) PL spectra of two QDs in separate nanowires on different piezoelectric substrates. (d) and (e) show the fluorescence lifetime measurements on the excitons for nanowire 1 and 2, respectively. Red lines are the fit functions consisting of an exponential decay convoluted with the detector response function. Reprinted from Ref. [70], with the permission of AIP Publishing.

entangled photons from QDs. However, reducing the exciton FSS by strain also results in a change of the QD emission wavelength. For the application of such sources in quantum information networks, wavelength-tunable entangled photon emission has to be demonstrated to ensure the indistinguishability of photons from separate emitters.

Fig. 12 shows a strain tunable quantum dot entangled photon source which fulfills that task. The emission wavelength and FSS can be tuned independently by strain applied along two orthogonal directions of a thin film of PMN-PT integrated on a silicon substrate. Fig. 12(a) represents a vision to employ such a technique in the novel micro-electromechanical system (MEMS) devices[138–141]. GaAs nanomembranes with InGaAs/GaAs QDs are transferred on the patterned piezoelectric substrate (Figs. 12(a)–12(c)). With two independent pairs of electrodes ("legs") A–C and B–D, the QDs emission wavelength and FSS can be adjusted independently (Figs. 12(d)–12(e)).

An example of such tuning is shown in Fig. 13. The voltage applied to B and D are fixed while the voltage V_{AC} is swept from 0 to 100 V (Figs. 13(a)–13(b)). The FSS first decreases monotonically to a minimum value and then increases again. The phase, angle between the X photon polarization and [1$\bar{1}$0] crystal direction experiences a sharp drop around the position where the FSS approaches a minimum, which is in agreement with theoretical prediction[142]. Except for the FSS tuning, the wavelength variation is also observed when the V_{BD} is fixed. The QD emission wavelength undergoes a linear decrease when sweeping V_{AC} from 0 to 100 V. In the meantime, zero FSSs are also obtained at different V_{AC}, indicating that FSS close to zero can be achieved at different emission wavelengths by using a suitable combination of V_{AC} and V_{BD} (Fig. 13(c)). Fig. 13(d) shows the different strain combinations along A–C and B–D, from where we can see the linear track of minimal FSS. Therefore, V_{BD} can be scanned to tune the emission wavelength, and then V_{AC} is adjusted to find minimal FSS.

Finally, the ability to eliminate the FSS at different X emission wavelengths is verified (Fig. 14(a)). While setting V_{BD} to values between 25 and –100 V, different emission wavelengths are obtained in combination with FSSs below 1 μeV. To further test the entangled photon fidelity, polarization-dependent cross-correlation measurements are performed. An entanglement fidelity of 0.73 is obtained, clearly above the classical limit of 0.5. Thereby, a silicon-integrated strain-tunable QD based source of polarization-entangled photons has been realized which allows for wavelength tuning of the entangled pairs.

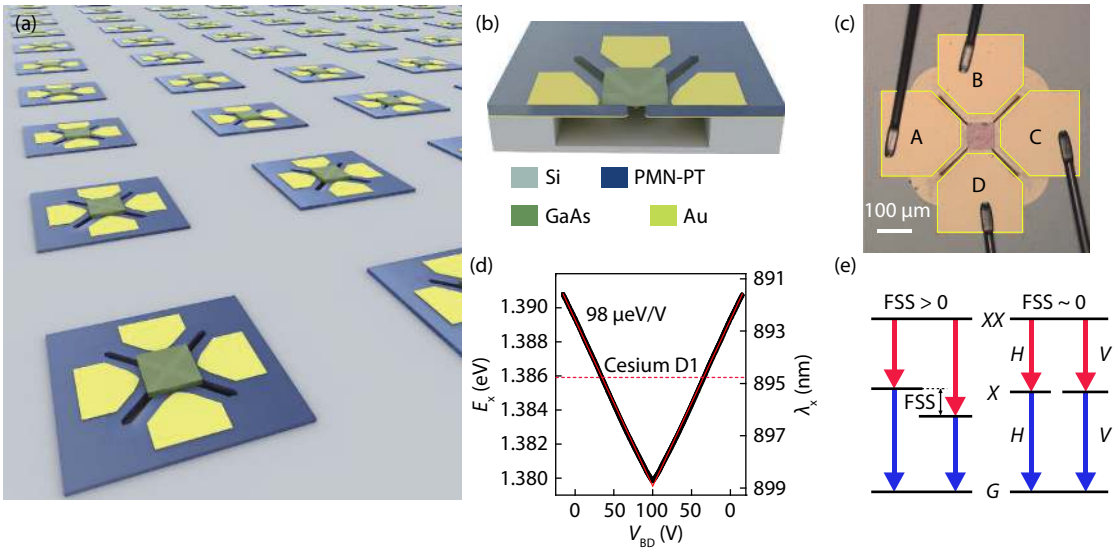

Fig. 12. (Color online) Silicon-based wavelength-tunable entangled photon source. (a) The vision of large scale integration of wavelength-tunable sources on silicon chips. (b) Sketch of the device. Focused ion beam (FIB) is used to create trenches on the PMN-PT surface and chemical etching is performed to suspend the different parts. A nanomembrane is then transferred to the top center of the four "legs". (c) microscope image of the device, showing the electric contacts on the legs A, B, C, and D, obtained by wire bonding. (d) Tuning of the QD emission wavelength with the applied voltage V_{BD} on PMN-PT. (e) Sketch of the biexciton cascade and the possibility of reducing the FSS in the QDs by strain. Figure is taken from Ref. [39] without changes are made. CC BY[119].

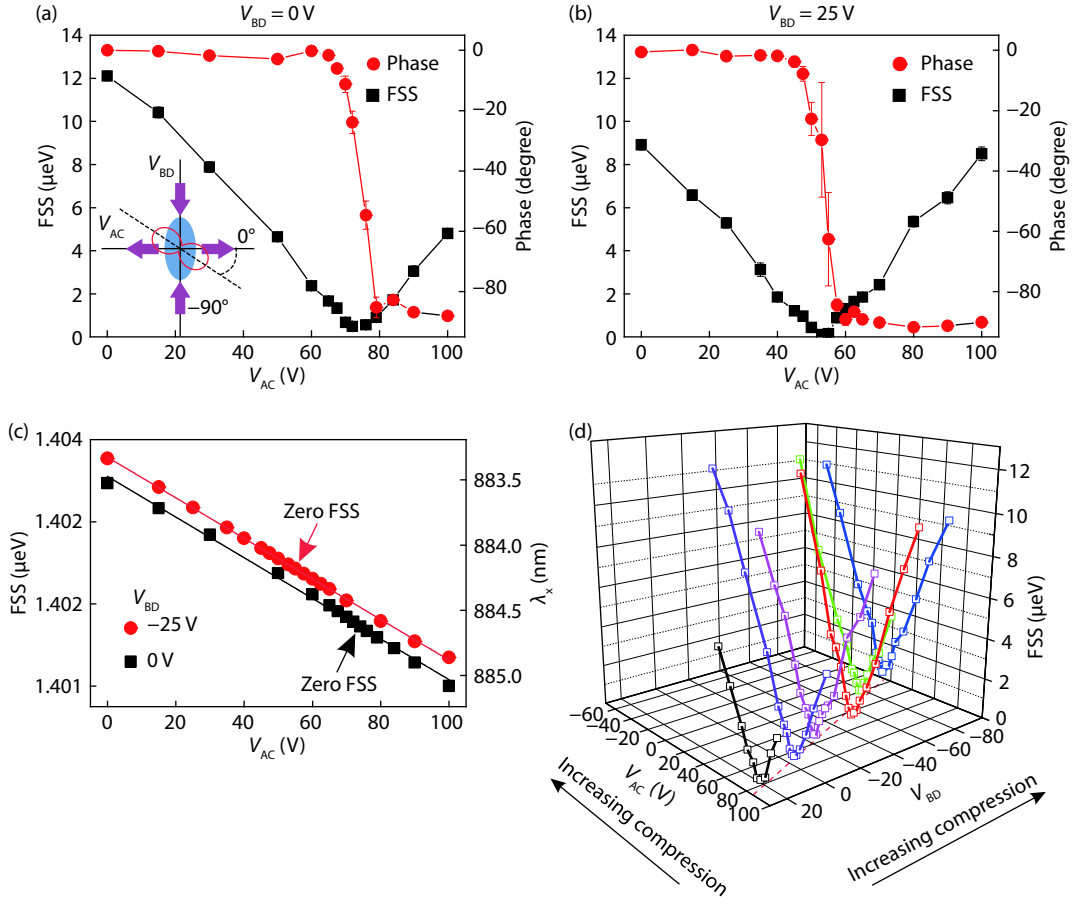

Fig. 13. (Color online) (a) and (b) show the strain-induced changes in FSS and polarization angle of *X* photons relative with the QD principal axis. The voltage is applied on legs A and C and the voltages on legs B and D are fixed at 0 and −25 V respectively. The ellipse in the inset indicates the asymmetric quantum dot confinement potential and the red solid line indicates the *X* photon polarization direction. (c) The *X* photon emission wavelength changes as a function of the voltage V_{AC} with two different fixed voltages V_{BD} at 0 V and −25 V. (d) The change of FSS while altering the strain in the QD along with two orthogonal directions (A–C and B–D). The dashed line indicates the track of minimal FSS with different strain combinations. Figure is taken from Ref. [39] without changes are made. CC BY[119].

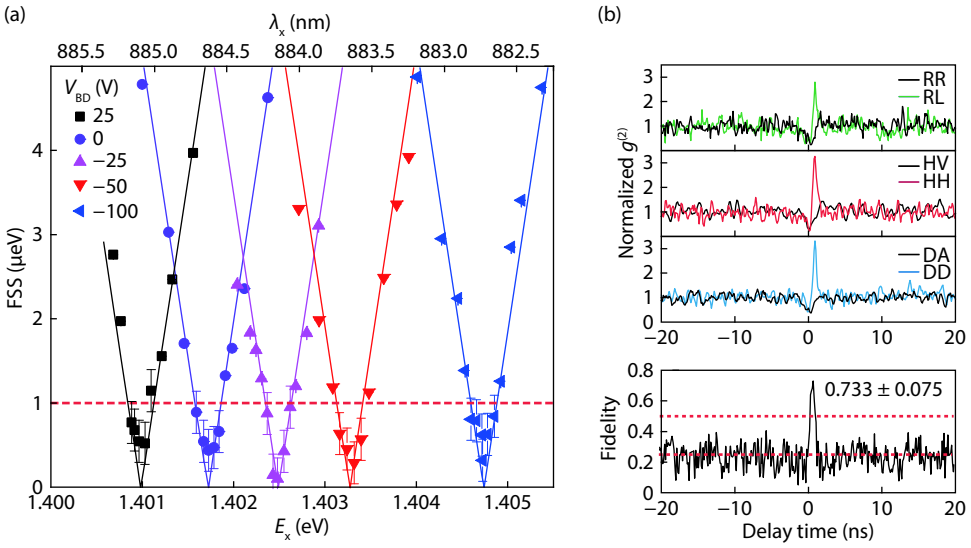

Fig. 14. (Color online) Simultaneous tuning of wavelength and fine structure splitting. (a) FSS of a single QD varies as a function of the tunable emission wavelength. A series of V_{BD} with a step size of 25 V from 25 to −100 V are investigated, while the voltage V_{AC} is changed at the same time to adjust the FSS. The red dashed line at FSS = 1 μeV implies the FSS limit for generating entangled photon pairs from the QD. (b) Polarization-dependent cross-correlation measurements on *XX* and *X* photons are performed and an entangle ement fidelity $f^+ = 0.733 \pm 0.075$ is obtained. Figure is taken from Ref. [39] without changes are made. CC BY[119].

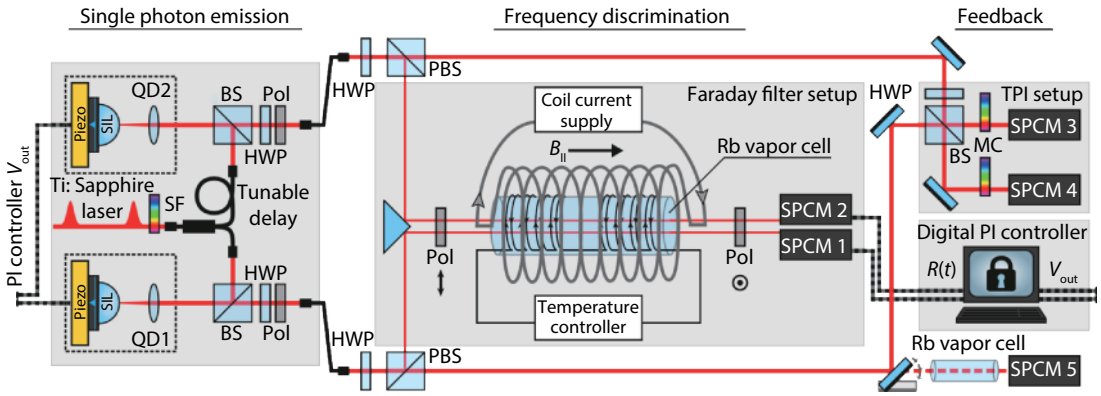

Fig. 15. (Color online) Experimental setup for Hong-Ou-Mandel interference with photons from separated and frequency stabilized quantum dots. A grating-based spectrum filter (SF) is used to filter the Ti: Sapphire excitation laser for resonant excitation of the biexciton state. The QDs containing membranes are placed on piezoelectric actuators in the 4 K environment and covered with a solid immersion lens (SIL) to enhance the brightness. The emitted photons from QD1 and QD2 are sent to a frequency discrimination setup. Parts of the photon streams from both QDs are sent to the Faraday filter setup via the half-wave plate (HWP) and the polarizing beam splitter. The faraday filter setup consists of a heated rubidium vapor cell in a longitudinal magnetic field and two crossed polarizers in front and behind the cell. Photons are then detected by single-photon counting modules 1 and 2 (SPCM1 and SPCM2). The estimated photon rates are used by a digital PI controller to apply feedback on the voltage applied to the piezoelectric actuators. Thereby the interference visibility is stabilized in the subsequent Hong-Ou-Mandel experiment. Reprinted figure with permission from Ref. [78]. Copyright (2019) by the American Physical Society.

8. Frequency feedback for strain tuning

Strain tuning can reversibly alter the wavelength and fine structure of QDs for their application as single or entangled photon sources, as discussed above. Long-term stable and reliable indistinguishability of separate QDs based photon emitters is another step to the real-world application[143, 144]. To counteract drifts in the emission features induced e.g. by piezo creep, frequency feedback[145–147] has to be employed.

Stabilizing the frequency of single-photon streams has been successfully realized using strain-tunable QD sources and a feedback system based on the transmission of rubidium based Faraday filter as a frequency reference. As a result, stable Hong-Ou-Mandel interference between photons from two separate QDs can be demonstrated (Fig. 15). First, part of the *XX* photon stream from each source is guided to a frequency discriminator, in this case, a rubidium-based Faraday filter. It consists of a heated rubidium vapor cell in a longitudinal magnetic field, sandwiched by two crossed polarizers. Subsequent single-photon detection, an efficient rate estimation algorithm, and a digital PI controller allow for the generation of an error signal. Thus, the corresponding tuning voltage is adapted for the piezo-substrates which carry the QD nanomembranes. In the experiment, the two QDs (1 and 2) are both excited via resonant two-photon excitation of the biexciton state.

In the experiment, the *XX* photon emission wavelengths

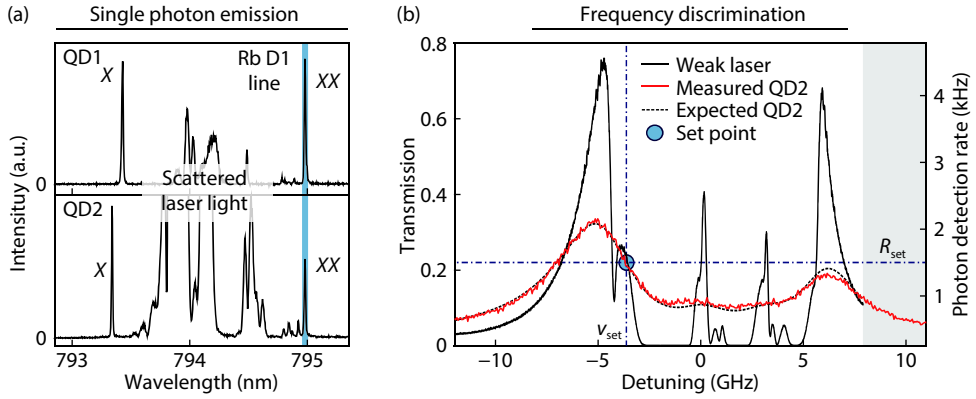

Fig. 16. (Color online) (a) Emission spectrum of QD1 and QD2. Two-photon resonant π pulse excitation is used and the two *XX* photon emissions are tuned into resonance with the rubidium D1 transitions. (b) Faraday filter transmission for a weak and narrow-band laser (black solid line) and frequency-tuned QD2 (red line). The convolution of the laser transmission and QD2 emission profile is used to model the QD transmission (black dash line). The setpoint for frequency feedback is highlighted. Reprinted figure with permission from Ref. [78]. Copyright 2019, the American Physical Society.

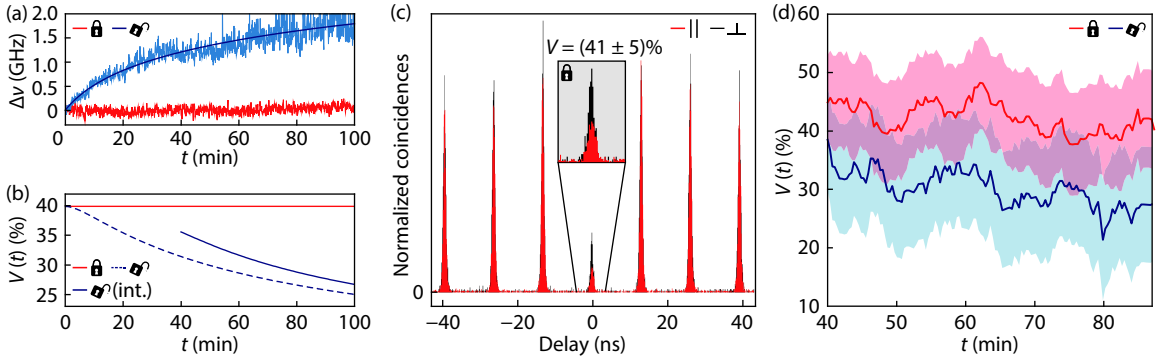

Fig. 17. (Color online) Frequency feedback for stable Hong-Ou-Mandel interference. (a) Emission wavelength drifts over time for the frequency stabilized (red line) and free-running mode (blue line). (b) Estimated Hong-Ou-Mandel interference visibility over time, imagining frequency drifts as determined in (a). The red line (blue dash line) shows the estimated visibility with (without) frequency feedback. The blue solid line represents the free-running mode of the QD emission with an integration time as used in the experiment. (c) Second-order correlation measurement after Hong-Ou-Mandel interference at a beam splitter. The red (black) coincidences are obtained for parallel (orthogonal) *XX* photon polarizations at the beam splitter. (d) Hong-Ou-Mandel interference visibility over time with (red) and without (blue) frequency feedback. The visibility for stabilized emission is always higher than for the free-running mode. The shaded areas represent the uncertainty of visibility based on Poissonian counting statistics. Reprinted figure with permission from Ref. [78]. Copyright 2019, the American Physical Society.

from both sources are tuned into resonance by the piezo-actuators. Then, two-photon excitation is used for both QDs so that a pure and deterministic *XX* emission is obtained[122, 148]. Fig. 16(a) shows the PL spectrum of QD1 and QD2, in which the laser emission is partially suppressed by notch filters. Fig. 16(b) shows the transmission of the Faraday filter for a narrow-band laser and the photons from QD2. The frequency set point is marked on the QD emission transmission curve. Frequency deviations due to piezo creep translate to count rate fluctuations, which are detected by SPCMs. A digital PI controller then adapts the strain tuning to the QDs nanomembrane on the piezo crystal by changing the voltage applied to the PMN-PT substrates[60].

From Fig. 17(a), it can be seen that the frequency keeps stable for the frequency-locked case (red line). For the free-running mode, the QD emission frequency strongly increases with the time, which can be fitted with a logarithmic function in agreement with the displacement change induced by piezo creep[77]. Now, the effect of frequency feedback to Hong-Ou-Mandel interference with photons from the separate QDs is investigated. Assuming frequency drifts as in Fig. 17(a), the interference visibility is estimated for both the frequency-locked and free-running case (Fig. 17(b)). Here, the experimentally determined lifetimes T_1 and coherence times T_2 from both QDs are used to model the visibility[149]. The visibility with applied frequency feedback is expected to be constant since the two *XX* photon emission frequencies keep in resonance (red solid line). For the free-running model, the visibility drops significantly with time (blue dash line). The visibility measurement is implemented by sending the *XX* photon from each QD to one of the two non-polarizing beam splitter input ports. By setting the input photon polarization to be parallel or perpendicular, the bunching (black field in Fig. 17(c)) and anti-bunching (red field in Fig. 17(c)) at zero-time delay are observed in the second-order correlations. Then the interference visibility is determined from the coincidences at zero delays for the two different polarization cases. As shown in Fig. 17(d), the long-term stability of the interference over time is tested. With applied frequency feedback, the interference visibility constantly keeps above the case

with free-running QDs. Furthermore, the interference visibility reached the maximum value for the employed QD emission and depends solely on the internal dephasing in the dots. Therefore, an efficient method to stabilize the frequency of photons emitted by remote QDs is demonstrated, which can find application in future quantum networks.

9. Conclusion

QDs are a promising candidate to fulfill the 'wish-list' for quantum information applications based on single- and entangled photons. They can overcome the fundamental limitation of SPDCs by emitting photons deterministically and on-demand. The integrability with semiconductor technology allows for a stable and scalable application in future quantum networks. Post-growth tuning via thermal annealing, electric or magnetic fields can compensate for the differences in photon properties inferred from randomness in the QD growth. However, drawbacks like reversibility, simplicity or flexibility reduce their applicability. In contrast, strain tuning provides a highly versatile and scalable platform: QDs may be tuned on-chip, reversibly, anisotropically and in combination with electrical control. We illustrate the functionality of biaxial PMN-PT devices, allowing for QD emission wavelength tunability under optical and electric excitation. The achievement of a wavelength-tunable light hole exciton emission is discussed. To successfully generate polarization-entangled photon pairs, uniaxial tuning with a PMN-PT actuator is applied to reduce the exciton FSS and restore the degeneracy. Wavelength-tunable entangled photon sources are obtained by microstructured, silicon-integrated piezo actuators, allowing for controlled anisotropic strain tuning. At last, the strain tunable emission wavelength of separate sources is stabilized by frequency feedback and long-term stability of a two-photon interference experiment illustrated. Based on the presented developments, the strain tuning of QDs is a scalable, versatile and reliable technique that may become a cornerstone for optical quantum information applications.

Several challenges remain for the practical application of such sources. The strain tuning platforms need to be extended for arrays of individual QDs or on-chip nanostructures. Furthermore, combining anisotropic strain tuning with LED structures or charge-tunable devices in order to ensure wavelength-tunability in combination with electrical injection or high photon coherence. Anisotropic strain tuning platforms may require feedback to be applied for maintaining a reduced FSS and constant emission wavelength simultaneously. Besides, strain tuning is also a viable approach for the optimization and development of other material systems such as color centers, 2D materials, molecules and so on. It can be therefore used as a tool to obtain a fundamental understanding of novel materials and to tune their properties for desired applications.

Acknowledgment

The work was financially supported by the ERC Starting Grant No. 715770 (QD-NOMS) and the National Natural Science Foundation of China (No. 61728501).

References

[1] Briegel H J, Dür W, Cirac J I, et al. Quantum repeaters: The role of imperfect local operations in quantum communication. Phys Rev Lett, 1998, 81(26), 5932

[2] Simon C, de Riedmatten H, Afzelius M, et al. Quantum repeaters with photon pair sources and multimode memories. Phys Rev Lett, 2007, 98(19), 190503

[3] Sangouard N, Simon C, de Riedmatten H, et al. Quantum repeaters based on atomic ensembles and linear optics. Rev Mod Phys, 2011, 83(1), 33

[4] Kok P, Munro W J, Nemoto K, et al. Linear optical quantum computing with photonic qubits. Rev Mod Phys, 2007, 79(1), 135

[5] Knill E, Laflamme R, Milburn G J. A scheme for efficient quantum computation with linear optics. Nature, 2001, 409(6816), 46

[6] Gisin N, Ribordy G, Tittel W, et al. Quantum cryptography. Rev Mod Phys, 2002, 74(1), 145

[7] Ekert A K. Quantum cryptography based on Bell's theorem. Phys Rev Lett, 1991, 67(6), 661

[8] Dowling J P, Seshadreesan K P. Quantum optical technologies for metrology, sensing, and imaging. J Lightwave Technol, 2015, 33(12), 2359

[9] Giovannetti V, Lloyd S, Maccone L. Quantum metrology. Phys Rev Lett, 2006, 96(1), 010401

[10] Afek I, Ambar O, Silberberg Y. High-NOON states by mixing quantum and classical light. Science, 2010, 328(5980), 879

[11] Schumacher B. Quantum coding. Phys Rev A, 1995, 51(4), 2738

[12] Bennett C H, Brassard G, Popescu S, et al. Purification of noisy entanglement and faithful teleportation via noisy channels. Phys Rev Lett, 1996, 76(5), 722

[13] Deutsch D, Ekert A, Jozsa R, et al. Quantum privacy amplification and the security of quantum cryptography over noisy channels. Phys Rev Lett, 1996, 77(1), 2818

[14] Burnham D C, Weinberg D L. Observation of simultaneity in parametric production of optical photon pairs. Phys Rev Lett, 1970, 25(2), 84

[15] Shih Y H, Alley C O. New type of Einstein-Podolsky-Rosen-Bohm experiment using pairs of light quanta produced by optical parametric down conversion. Phys Rev Lett, 1988, 61(26), 2921

[16] Kwiat P G, Mattle K, Weinfurter H, et al. New high-intensity source of polarization-entangled photon pairs. Phys Rev Lett, 1995, 75(24), 4337

[17] Bennett C H, Brassard G, Crépeau C, et al. Teleporting an unknown quantum state via dual classical and Einstein-Podolsky-Rosen channels. Phys Rev Lett, 1993, 70(13), 1895

[18] Vaidman L. Teleportation of quantum states. Phys Rev A, 1994, 49(2), 1473

[19] Bouwmeester D, Pan J W, Mattle K, et al. Experimental quantum teleportation. Nature, 1997, 390(6660), 575

[20] Boschi D, Branca S, De Martini F, et al. Experimental realization of teleporting an unknown pure quantum state via dual classical and Einstein-Podolsky-Rosen channels. Phys Rev Lett, 1998, 80(6), 1121

[21] Nilsson J, Stevenson R M, Chan M H A, et al. Quantum teleportation using a light-emitting diode. Nat Photonics, 2013, 7(4), 311

[22] Huwer J, Stevenson R M, Skiba-Szymanska J, et al. Quantum-dot-based telecommunication-wavelength quantum relay. Phys Rev Appl, 2017, 8(2), 1

[23] Żukowski M, Zeilinger A, Horne M A, et al. "Event-ready-detectors" bell experiment via entanglement swapping. Phys Rev Lett, 1993, 71(26), 4287

[24] Pan J W, Bouwmeester D, Weinfurter H, et al. Experimental entanglement swapping: entangling photons that never interacted. Phys Rev Lett, 1998, 80(18), 3891

[25] Sun Q C, Mao Y L, Jiang Y F, et al. Entanglement swapping with independent sources over an optical-fiber network. Phys Rev A, 2017, 95(3), 32306

[26] Zhang Y, Agnew M, Roger T, et al. Simultaneous entanglement swapping of multiple orbital angular momentum states of light.

Nat Commun, 2017, 8(1), 1
[27] Pan J W, Simon C, Brukner Č, et al. Entanglement purification for quantum communication. Nature, 2001, 410(6832), 1067
[28] Bouwmeester D, Pan J W, Bongaerts M, et al. Observation of three-photon greenberger-horne-zeilinger entanglement. Phys Rev Lett, 1999, 82(7), 1345
[29] Zhang C, Huang Y F, Liu B H, et al. Experimental generation of a high-fidelity four-photon linear cluster state. Phys Rev A, 2016, 93(6), 062329
[30] Pan J W, Daniell M, Gasparoni S, et al. Experimental demonstration of four-photon entanglement and high-fidelity teleportation. Phys Rev Lett, 2001, 86(20), 4435
[31] Lu C Y, Zhou X Q, Gühne O, et al. Experimental entanglement of six photons in graph states. Nat Phys, 2007, 3(2), 91
[32] Michler P, Kiraz A, Becher C, et al. A quantum dot single-photon turnstile device. Science, 2000, 290(5500), 2282
[33] Michler P, Imamoğlu A, Mason M D, et al. Quantum correlation among photons from a single quantum dot at room temperature. Nature, 2000, 406(6799), 968
[34] Radnaev A G, Dudin Y O, Zhao R, et al. A quantum memory with telecom-wavelength conversion. Nat Phys, 2010, 6(11), 894
[35] Chanelière T, Matsukevich D N, Jenkins S D, et al. Quantum telecommunication based on atomic cascade transitions. Phys Rev Lett, 2006, 96(9), 093604
[36] Stevenson R M, Young R J, Atkinson P, et al. A semiconductor source of triggered entangled photon pairs. Nature, 2006, 439(7073), 179
[37] Bennett A J, Pooley M A, Stevenson R M, et al. Electric-field-induced coherent coupling of the exciton states in a single quantum dot. Nat Phys, 2010, 6(12), 947
[38] Salter C L, Stevenson R M, Farrer I, et al. An entangled-light-emitting diode. Nature, 2010, 465(7298), 594
[39] Chen Y, Zhang J, Zopf M, et al. Wavelength-tunable entangled photons from silicon-integrated III–V quantum dots. Nat Commun, 2016, 7, 10387
[40] Harris N C, Grassani D, Simbula A, et al. Integrated source of spectrally filtered correlated photons for large-scale quantum photonic systems. Phys Rev X, 2014, 4(4), 041047
[41] Zopf M, Keil R, Chen Y, et al. Entanglement swapping with semiconductor-generated photons. Phys Rev Lett, 2001, 9, 123
[42] Rogers L J, Jahnke K D, Teraji T, et al. Multiple intrinsically identical single-photon emitters in the solid state. Nat Commun, 2014, 5(1), 4379
[43] Morfa A J, Gibson B C, Karg M, et al. Single-photon emission and quantum characterization of zinc oxide defects. Nano Lett, 2012, 12(2), 949
[44] Kurtsiefer C, Mayer S, Zarda P, et al. Stable solid-state source of single photons. Phys Rev Lett, 2000, 85(2), 290
[45] Simpson D A, Ampem-Lassen E, Gibson B C, et al. A highly efficient two level diamond based single photon source. App Phys Lett, 2009, 94(20), 203107
[46] Aharonovich I, Englund D, Toth M. Solid-state single-photon emitters. Nat Photon, 2016, 10(10), 631
[47] Boyd R W, Lukishova S G, Zadkov V N. Quantum photonics: pioneering advances and emerging applications. Springer, 2019
[48] Michler P. Single semiconductor quantum dots. Berlin Heidelberg: Springer-Verlag, 2009
[49] Dupertuis M A, Karlsson K F, Oberli D Y, et al. Symmetries and the polarized optical spectra of exciton complexes in quantum dots. Phys Rev Lett, 2011, 107(12), 127403
[50] Bayer M, Ortner G, Stern O, et al. Fine structure of neutral and charged excitons in self-assembled In(Ga)As/(Al)GaAs quantum dots. Phys Rev B, 2002, 65(19), 195315
[51] Stevenson R M, Hudson A J, Bennett A J, et al. Evolution of entanglement between distinguishable light states. Phys Rev Lett, 2008, 101(17), 170501
[52] Trotta R, Wildmann J S, Zallo E, et al. Highly entangled photons from hybrid piezoelectric-semiconductor quantum dot devices. Nano Lett, 2014, 14(6), 3439
[53] Hudson A J, Stevenson R M, Bennett A J, et al. Coherence of an entangled exciton-photon state. Phys Rev Lett, 2007, 99(26), 266802
[54] Keil R, Zopf M, Chen Y, et al. Solid-state ensemble of highly entangled photon sources at rubidium atomic transitions. Nat Commun, 2017, 8, 15501
[55] Kiravittaya S, Lee H S, Balet L, et al. Tuning optical modes in slab photonic crystal by atomic layer deposition and laser-assisted oxidation. J Appl Phys, 2011, 109(5), 053115
[56] Ellis D J P, Stevenson R M, Young R J, et al. Control of fine-structure splitting of individual InAs quantum dots by rapid thermal annealing. Appl Phys Lett, 2007, 90(1), 011907
[57] Pooley M A, Bennett A J, Stevenson R M, et al. Energy-tunable quantum dot with minimal fine structure created by using simultaneous electric and magnetic fields. Phys Rev Appl, 2014, 1(2), 024002
[58] Ghali M, Ohtani K, Ohno Y, et al. Generation and control of polarization-entangled photons from GaAs island quantum dots by an electric field. Nat Commun, 2012, 3, 661
[59] Muller A, Fang W, Lawall J, et al. Creating polarization-entangled photon pairs from a semiconductor quantum dot using the optical stark effect. Phys Rev Lett, 2009, 103(21), 217402
[60] Ding F, Singh R, Plumhof J D, et al. Tuning the exciton binding energies in single self-assembled InGaAs/GaAs quantum dots by piezoelectric-induced biaxial stress. Phys Rev Lett, 2010, 104(6), 2
[61] Zhang J, Ding F, Zallo E, et al. A nanomembrane-based wavelength-tunable high-speed single-photon-emitting diode. Nano Lett, 2013, 13(12), 5808
[62] Zhang J, Zallo E, Höfer B, et al. Electric-field-induced energy tuning of on-demand entangled-photon emission from self-assembled quantum dots. Nano Lett, 2017, 17(1), 501
[63] Zhang J, Huo Y, Ding F, et al. Energy-tunable single-photon light-emitting diode by strain fields. Appl Phys B, 2016, 122(1), 1
[64] Höfer B, Zhang J, Wildmann J, et al. Independent tuning of excitonic emission energy and decay time in single semiconductor quantum dots. Appl Phys Lett, 2017, 110(15), 151102
[65] Zhang J, Wildmann J S, Ding F, et al. High yield and ultrafast sources of electrically triggered entangled-photon pairs based on strain-tunable quantum dots. Nat Commun, 2015, 6, 10067
[66] Huo Y H, Witek B J, Kumar S, et al. A light-hole exciton in a quantum dot. Nat Phys, 2013, 10(1), 46
[67] Zhang J, Huo Y, Rastelli A, et al. Single photons on-demand from light-hole excitons in strain-engineered quantum dots. Nano Lett, 2015, 15(1), 422
[68] Wang J, Gong M, Guo G C, et al. Towards scalable entangled photon sources with self-assembled InAs/GaAs quantum dots. Phys Rev Lett, 2015, 115(6), 067401
[69] Trotta R, Martín-Sánchez J, Daruka I, et al. Energy-tunable sources of entangled photons: a viable concept for solid-state-based quantum relays. Phys Rev Lett, 2015, 114(15), 150502
[70] Chen Y, Zadeh I E, Jöns K D, et al. Controlling the exciton energy of a nanowire quantum dot by strain fields. Appl Phys Lett, 2016, 108(18), 182103
[71] Versteegh M A M, Reimer M E, Jöns K D, et al. Observation of strongly entangled photon pairs from a nanowire quantum dot. Nat Commun, 2014, 5, 5298
[72] Bulgarini G, Reimer M E, Bavinck M B, et al. Nanowire waveguides launching single photons in a Gaussian mode for ideal fiber coupling. Nano Lett, 2014, 14, 1428
[73] Davanço M, Rakher M T, Schuh D, et al. A circular dielectric grating for vertical extraction of single quantum dot emission. Appl Phys Lett, 2011, 99(4), 041102

[74] Liu J, Su R, Wei Y, et al. A solid-state source of strongly entangled photon pairs with high brightness and indistinguishability. Nat Nanotechnol, 2019, 14(6), 586
[75] Wang H, Hu H, Chung T H, et al. On-demand semiconductor source of entangled photons which simultaneously has high fidelity, efficiency, and indistinguishability. Phys Rev Lett, 2019, 122(11), 113602
[76] Moczała-Dusanowska M, Dusanowski Ł, Gerhardt S, et al. Strain-tunable single-photon source based on a quantum dot–micropillar system. ACS Photonics, 2019, 6(8), 2025
[77] Jung H, Gweon D G. Creep characteristics of piezoelectric actuators. Rev Sci Instrum, 2000, 71(4), 1896
[78] Zopf M, Macha T, Keil R, et al. Frequency feedback for two-photon interference from separate quantum dots. Phys Rev B, 2018, 98(16), 161302
[79] Chuang S L. Physics of photonic devices. Hoboken, NJ: Wiley, 2009
[80] Pikus G E. Effect of deformation on the hole energy spectrum of germanium and silicon. Sov Phys-Solid State, 1960, 11502
[81] Bir G L, Pikus G E. Symmetry and strain-induced effects in semiconductors. New York: Wiley, 1974
[82] Trotta R, Atkinson P, Plumhof J D, et al. Nanomembrane quantum-light-emitting diodes integrated onto piezoelectric actuators. Adv Mater, 2012, 24(20), 2668
[83] Kumar S, Trotta R, Zallo E, et al. Strain-induced tuning of the emission wavelength of high quality GaAs/AlGaAs quantum dots in the spectral range of the ^{87}Rb D_2 lines. Appl Phys Lett, 2011, 99(16), 161118
[84] Plumhof J D, Trotta R, Křápek V, et al. Tuning of the valence band mixing of excitons confined in GaAs/AlGaAs quantum dots via piezoelectric-induced anisotropic strain. Phys Rev B, 2013, 87(7), 075311
[85] Benson O, Santori C, Pelton M, et al. Regulated and entangled photons from a single quantum dot. Phys Rev Lett, 2000, 84(11), 2513
[86] Ward M B, Dean M C, Stevenson R M, et al. Coherent dynamics of a telecom-wavelength entangled photon source. Nat Commun, 2014, 5(1), 3316
[87] Santori C, Fattal D, Pelton M, et al. Polarization-correlated photon pairs from a single quantum dot. Phys Rev B, 2002, 66(4), 045308
[88] Stevenson R M, Thompson R M, Shields A J, et al. Quantum dots as a photon source for passive quantum key encoding. Phys Rev B, 2002, 66(8), 081302
[89] Bester G. Electronic excitations in nanostructures: an empirical pseudopotential based approach. J Phys: Condens Matter, 2008, 21(2), 023202
[90] Ding F, Ji H, Chen Y, et al. Stretchable graphene: a close look at fundamental parameters through biaxial straining. Nano Lett, 2010, 10(9), 3453
[91] Zallo E, Trotta R, Křápek V, et al. Strain-induced active tuning of the coherent tunneling in quantum dot molecules. Phys Rev B, 2014, 89(24), 241303
[92] Meesala S, Sohn Y I, Pingault B, et al. Strain engineering of the silicon-vacancy center in diamond. Phys Rev B, 2018, 97(20), 205444
[93] Kiršanskė G, Thyrrestrup H, Daveau R S, et al. Indistinguishable and efficient single photons from a quantum dot in a planar nanobeam waveguide. Phys Rev B, 2017, 96(16), 165306
[94] Lodahl P. Quantum-dot based photonic quantum networks. Quantum Sci Technol, 2017, 3(1), 013001
[95] Daveau R S, Balram K C, Pregnolato T, et al. Efficient fiber-coupled single-photon source based on quantum dots in a photonic-crystal waveguide. Optica, 2017, 4(2), 178
[96] Pan J W, Gasparoni S, Ursin R. Experimental entanglement purification of arbitrary unknown states. Nature, 2003, 423, 417
[97] Chen L K, Yong H L, Xu P, et al. Experimental nested purification for a linear optical quantum repeater. Nat Photon, 2017, 11(11), 695
[98] Sheng Y B, Zhou L, Long G L. Hybrid entanglement purification for quantum repeaters. Phys Rev A, 2013, 88(2), 022302
[99] de Riedmatten H, Marcikic I, Tittel W, et al. Long distance quantum teleportation in a quantum relay configuration. Phys Rev Lett, 2004, 92(4), 047904
[100] Bennett A J, Unitt D C, See P, et al. Electrical control of the uncertainty in the time of single photon emission events. Phys Rev B, 2005, 72(3), 033316
[101] Reischle M, Kessler C, Schulz W M, et al. Triggered single-photon emission from electrically excited quantum dots in the red spectral range. Appl Phys Lett, 2010, 97(14), 143513
[102] Hargart F, Kessler C A, Schwarzbäck T, et al. Electrically driven quantum dot single-photon source at 2 GHz excitation repetition rate with ultra-low emission time jitter. Appl Phys Lett, 2013, 102(1), 011126
[103] Troncale V, Karlsson K F, Pelucchi E, et al. Control of valence band states in pyramidal quantum dot-in-dot semiconductor heterostructures. Appl Phys Lett, 2007, 91(24), 241909
[104] Karlsson K F, Dupertuis M A, Oberli D Y, et al. Fine structure of exciton complexes in high-symmetry quantum dots: Effects of symmetry breaking and symmetry elevation. Phys Rev B, 2010, 81(16), 161307
[105] Vrijen R, Yablonovitch E. A spin-coherent semiconductor photodetector for quantum communication. Physica E, 2001, 10(4), 569
[106] Sleiter D, Brinkman W F. Using holes in GaAs as qubits: An estimate of the Rabi frequency in the presence of an external RF field. Phys Rev B, 2006, 74(15), 153312
[107] Kosaka H, Inagaki T, Rikitake Y, et al. Spin state tomography of optically injected electrons in a semiconductor. Nature, 2009, 457(7230), 702
[108] L Besombes L, K Kheng K, Martrou D. Exciton and biexciton fine structure in single elongated islands grown on a vicinal surface. Phys Rev Lett, 2000, 85(2), 425
[109] Belhadj T, Amand T, Kunold A, et al. Impact of heavy hole-light hole coupling on optical selection rules in GaAs quantum dots. Appl Phys Lett, 2010, 97(5), 051111
[110] Zhou W, Shen H, Pamulapati J, et al. Heavy- and light-hole band crossing in a variable-strain quantum-well heterostructure. Phys Rev B, 1995, 51(8), 5461
[111] Zhou W, Shen H, J Pamulapati J, et al. Simultaneous blue- and red-shift of light-hole and heavy-hole band in a novel variable-strain quantum well heterostructure. Appl Phys Lett, 1995, 66(5), 607
[112] Huo Y H, Rastelli A, Schmidt O G. Ultra-small excitonic fine structure splitting in highly symmetric quantum dots on GaAs (001) substrate. Appl Phys Lett, 2013, 102(15), 152105
[113] Witek B J, Heeres R W, Perinetti U, et al. Measurement of the *g*-factor tensor in a quantum dot and disentanglement of exciton spins. Phys Rev B, 2011, 84(19), 195305
[114] Wang X L, Chen L K, W Li W, et al. Experimental ten-photon entanglement. Phys Rev Lett, 2016, 117(21), 210502
[115] Scarani V, de Riedmatten H, Marcikic I, et al. Four-photon correction in two-photon Bell experiments. Eur Phys J D, 2005, 32(1), 129
[116] Seidl S, Högele A, Kroner M, et al. Tuning the cross-gap transition energy of a quantum dot by uniaxial stress. Physica E, 2006, 32(1), 14
[117] Bryant G W, Zieliński M, N Malkova N, et al. Effect of mechanical strain on the optical properties of quantum dots: controlling exciton shape, orientation, and phase with a mechanical strain. Phys Rev Lett, 2010, 105(6), 067404
[118] Michler P. Quantum dots for quantum information technolo-

gies. Springer International Publishing, 2017
[119] Creative Commons Attribution 4.0 International License. http://creativecommons.org/licenses/by/4.0/.
[120] Gong M, Zhang W, Guo G C, et al. Exciton polarization, fine-structure splitting, and the asymmetry of quantum dots under uniaxial stress. Phys Rev Lett, 2011, 106(22), 227401
[121] Singh R, Bester G. Lower bound for the excitonic fine structure splitting in self-assembled quantum dots. Phys Rev Lett, 2010, 104(19), 196803
[122] Müller M, Bounouar S, Jöns K D, et al. On-demand generation of indistinguishable polarization-entangled photon pairs. Nat Photonics, 2014, 8(3), 224
[123] Altepeter J B, Jeffrey E R, Kwiat P G. Photonic state tomography. Adv Atom, Mol, Opt Phys, 2015, 52, 105
[124] James D F V, Kwiat P G, Munro W J, et al. Measurement of qubits. Phys Rev A, 2001, 64(5), 052312
[125] Dousse A, Suffczyński J, Beveratos A, et al. Ultrabright source of entangled photon pairs. Nature, 2010, 466(7303), 217
[126] Chen Y, Zopf M, Keil R, et al. Highly-efficient extraction of entangled photons from quantum dots using a broadband optical antenna. Nat Commun, 2018, 9(1), 1
[127] Kuhn A, Hennrich M, Rempe G. Deterministic single-photon source for distributed quantum networking. Phys Rev Lett, 2002, 89(6), 067901
[128] Flagg E B, Muller A, Polyakov S V, et al. Interference of single photons from two separate semiconductor quantum dots. Phys Rev Lett, 2010, 104(13), 137401
[129] Friedler I, Sauvan C, Hugonin J P, et al. Solid-state single photon sources: the nanowire antenna. Opt Express, 2009, 17(4), 2095
[130] Heindel T, Schneider C, Lermer M, et al. Electrically driven quantum dot-micropillar single photon source with 34% overall efficiency. Appl Phys Lett, 2010, 96(1), 011107
[131] Reimer M E, Bulgarini G, Akopian N, et al. Bright single-photon sources in bottom-up tailored nanowires. Nat Commun, 2012, 3, 737
[132] Bulgarini G, D Dalacu D, P J Poole P J, et al. Far field emission profile of pure wurtzite InP nanowires. Appl Phys Lett, 2014, 105(19), 191113
[133] Gregersen N, Nielsen T R, Claudon J, et al. Controlling the emission profile of a nanowire with a conical taper. Opt Lett, OL, 2008, 33(15), 1693
[134] Dalacu D, Mnaymneh K, Lapointe J, et al. Ultraclean emission from InAsP quantum dots in defect-free wurtzite InP nanowires. Nano Lett, 2012, 12(11), 5919
[135] Reimer M E, Bulgarini G, Fognini A, et al. Overcoming power broadening of the quantum dot emission in a pure wurtzite nanowire. Phys Rev B, 2016, 93(19), 195316
[136] Signorello G, Karg S, Björk M T, et al. Tuning the light emission from GaAs nanowires over 290 meV with uniaxial strain. Nano Lett, 2013, 13(3), 917
[137] Kremer P E, Dada A C, Kumar P, et al. Strain-tunable quantum dot embedded in a nanowire antenna. Phys Rev B, 2014, 90(20), 201408
[138] A Politi A, Cryan M J, Rarity J G, et al. Silica-on-silicon waveguide quantum circuits. Science, 2008, 320(5876), 646
[139] Silverstone J W, Bonneau D, Ohira K, et al. On-chip quantum interference between silicon photon-pair sources. Nat Photonics, 2014, 8(2), 104
[140] Najafi N, Mower J, Harris N C, et al. On-chip detection of non-classical light by scalable integration of single-photon detectors. Nat Commun, 2015, 6, 5873
[141] O'Brien J L, Furusawa A, Vučković J. Photonic quantum technologies. Nat Photonics, 2009, 3(12), 687
[142] Plumhof J D, Křápek V, Ding F, et al. Strain-induced anticrossing of bright exciton levels in single self-assembled GaAs/$Al_xGa_{1-x}As$ and $In_xGa_{1-x}As$/GaAs quantum dots. Phys Rev B, 2011, 83(12), 121302
[143] Giesz V, Portalupi S L, Grange T, et al. Cavity-enhanced two-photon interference using remote quantum dot sources. Phys Rev B, 2015, 92(16), 161302
[144] Thoma A, Schnauber P, Böhm J, et al. Two-photon interference from remote deterministic quantum dot microlenses. Appl Phys Lett, 2017, 110(1), 011104
[145] Akopian N, Trotta R, Zallo E, et al. An artificial atom locked to natural atoms. ArXiv:13022005 [Cond-Mat, Physics:Physics, Physics:Quant-Ph], 2013
[146] Prechtel J H, Kuhlmann A V, Houel J, et al. Frequency-stabilized source of single photons from a solid-state qubit. Phys Rev X, 2013, 3(4), 041006
[147] Metcalfe M, Muller A, Solomon G S, et al. Active feedback of a Fabry-Perot cavity to the emission of a single InAs/GaAs quantum dot. J Opt Soc Am B, 2009, 26(12), 2308
[148] Brunner K, Abstreiter G, Böhm G, et al. Sharp-line photoluminescence and two-photon absorption of zero-dimensional biexcitons in a GaAs/AlGaAs structure. Phys Rev Lett, 1994, 73(8), 1138
[149] Bylander J, Robert-Philip I, Abram I. Interference and correlation of two independent photons. Eur Phys J D, 2003, 22(2), 295